

Dielectric and optical properties of epitaxial rare-earth scandate films and their crystallization behavior

H. M. Christen^{a)} and G. E. Jellison, Jr.

Materials Science and Technology Division, Oak Ridge National Laboratory, Oak Ridge, Tennessee 37831

I. Ohkubo

Department of Applied Chemistry, School of Engineering, University of Tokyo, Tokyo 113-8656, Japan

S. Huang and M. E. Reeves

Department of Physics, George Washington University, Washington, DC 20052

E. Cicerrella and J. L. Freeouf

Department of Physics, Portland State University, Portland, Oregon 97207

Y. Jia and D. G. Schlom

Department of Materials Science and Engineering, Pennsylvania State University, University Park, Pennsylvania 16802

(Received 6 January 2006; accepted 6 May 2006; published online 29 June 2006)

Rare-earth scandates ($ReScO_3$, with $Re=Y, La, Pr, Nd, Sm, Gd, Tb, Dy, Ho, Er, Tm, Yb,$ and Lu , i.e., the entire series for which the individual oxides are chemically stable in contact with Si) were deposited in a temperature-gradient pulsed laser deposition system onto $LaAlO_3$ substrates. The crystallization temperature depends monotonically on the Re atomic number and the Goldschmidt tolerance factor, with crystallization temperatures as low as $650^\circ C$ for $LaScO_3$ and $PrScO_3$. The dielectric constants of the crystalline films $K \approx 30$ (determined by microwave microscopy) are significantly larger than those of their amorphous counterparts. In combination with the large observed band gaps ($E_g > 5.5$ eV, determined by ellipsometry), these results indicate the potential of these materials as high- K dielectrics for field-effect transistor applications. © 2006 American Institute of Physics. [DOI: 10.1063/1.2213931]

The development of an alternative gate dielectric for future metal-oxide-semiconductor field-effect transistors (MOSFETs) on silicon remains a critical hurdle for the semiconductor industry. Candidate materials must simultaneously satisfy the criteria of a high dielectric constant K , chemical stability in contact with silicon under normal processing conditions,¹ and a large band gap and large band offsets relative to silicon (quantities that differ in general between crystalline and amorphous forms).

Several members of the family of rare-earth scandates ($ReScO_3$, where Re stands for Y, La, or a lanthanide) have been studied.² Dielectric constants K in the range of 18–35.5 (Ref. 3) and large optical band gaps^{4–6} (see Table I) are reported for single crystal $SmScO_3$, $GdScO_3$, $DyScO_3$, and $NdScO_3$, and epitaxial films of $LaScO_3$, $GdScO_3$, and $DyScO_3$ (with $K \sim 26, 20,$ and 22 , respectively) were recently grown onto $SrRuO_3/SrTiO_3$ substrates.⁷ Large optical band gaps⁸ and K values of ~ 22 (Ref. 9) were also observed on amorphous La-, Gd-, and Dy-scandate films.

A key issue for both amorphous and crystalline films is the crystallization temperature. In applications of amorphous high- K dielectrics, crystallization of the material during subsequent device processing must be avoided, whereas epitaxial (crystalline) films are technologically feasible only if the crystallization temperature is sufficiently low. Thus, in this letter, we report a systematic investigation of the crystallization temperatures of $ReScO_3$ thin films.

We apply our previously introduced temperature-gradient technique¹⁰ to systematically study the entire family

of known rare-earth scandates (with the exception of $EuScO_3$, which is not expected to be thermodynamically stable in direct contact with silicon¹¹), i.e., $Re=Y, La, Pr, Nd, Sm, Gd, Tb, Dy, Ho, Er, Tm, Yb,$ and Lu . The approach is based on pulsed laser deposition (248 nm radiation) in 80 mTorr of O_2 . In each deposition run of this particular temperature-gradient method, ten $LaAlO_3$ single crystalline, (012) [i.e., pseudocubic (001)]-oriented substrates are mounted onto a metallic plate, each heated to a different temperature (in $50^\circ C$ intervals between 350 and $800^\circ C$). Film thicknesses between 250 and 1000 nm were obtained in each 25 000-pulse run (depending on the target).

Simple x-ray θ - 2θ diffraction scans, recorded for all samples obtained in each deposition run, served as an approximate means to determine the films' crystallization temperature. We define an onset crystallization temperature by the first appearance of a film peak (poor crystallinity) and a temperature for complete crystallization (T_{cryst}) above which the film peak's components due to the $Cu K\alpha_1$ and $Cu K\alpha_2$ radiations are clearly separated (see Fig. 1). The crystallization temperatures determined this way are shown as a function of the A-site atomic number in Fig. 1(c). No x-ray peaks were observed for $TmScO_3$, $YbScO_3$, and $LuScO_3$, indicating either that the perovskite phase does not form or that it crystallizes only above $800^\circ C$.

No obvious relationship to the crystallization temperatures determined here (T_{cryst}) with the melting temperatures^{12,13} (T_m) listed in Table I is observed. Rather, T_{cryst} correlates well with the Goldschmidt tolerance factor $t = [(r_A + r_O) / (\sqrt{2}(r_B + r_O))]$, a conventional measure of stability for ABO_3 perovskites. (Here, r_A and r_B are the ionic radii

^{a)}Electronic mail: christenhm@ornl.gov

TABLE I. Properties of $ReScO_3$ films on $LaAlO_3$, compared to published values. a_{pc} (bulk) is calculated from the unit cell volume (Ref. 14 and 21). The tolerance factor t is calculated according to the text. T_{cryst} , d , K , n , and E_g refer to the crystallization temperature, thickness, dielectric constant at 1.7 GHz, refractive index, and direct optical band gap for the thin film samples. For the bulk dielectric constant K_{bulk} , all three tensor elements are given where available (measured at 1 MHz), and bulk E_g values correspond to high absorption band edges. Error bars for K are given in parentheses, and brackets indicate references. n/d indicates that no perovskite phase was detected by x-ray diffraction.

	Z	c_{film} (Å)	a_{pc} (bulk) (Å)	t	T_{cryst} (°C)	T_m (bulk) (°C)	d (nm)	K (this work)	K_{bulk} (Ref. 3)	n (400 nm)	E_g (this work) (eV)	E_g (bulk) (eV)
YScO ₃	39	3.962	3.940	0.816	n/d		500	20(1.5)				
LaScO ₃	57	4.050	4.053	0.863	650	2390 ^a	953	32(1.5)		2.11		
							400	32(1.2)		2.15	5.72	
PrScO ₃	59	4.024	4.022	0.850	650		1000	29(1.2)		2.15		
							350	30(2.0)		2.20	5.76	
NdScO ₃	60	4.014	4.011	0.845	700	2100 ^b	309	36(3.0)	23	2.15	5.52	
SmScO ₃	62	3.990	3.990	0.835	750	2100 ^b	372	37(3.1)	18	2.07	5.55	5.5–6.0 ^c
GdScO ₃	64	3.981	3.970	0.827	800	2100 ^b	705	31(2.0)	22.8, 19.2, 29.5	2.17	6.12	5.7 ^d
TbScO ₃	65	3.979	3.957	0.823	800		312	39(4.7)		2.11	5.61	
DyScO ₃	66	3.965	3.952	0.819	750	2100 ^a	215	31(2.1)	22, 18.8, 35.5	2.13	5.73, 5.95	5.7 ^d
HoScO ₃	67	3.967	3.943	0.815	800		226	32(5.5)			5.95	
ErScO ₃	68	3.967		0.812	>800		245	20(1.5)				
TmScO ₃	69			0.808	n/d							
YbScO ₃	70			0.805	n/d							
LuScO ₃	71			0.802	n/d							

^aReference 11.

^bReference 12.

^cReference 4.

^dReference 6.

of the A-site and B-site cations, respectively, r_O is the ionic radius of oxygen, and $t=1$ corresponds to a perfect perovskite arrangement.) As shown in Table I, for larger tolerance factors (approaching the value $t=1$), lower crystallization temperatures are observed.

For those scandates that crystallize below 800 °C in this study (La–Ho), bulk structural analysis shows an orthorhombic structure [space group $Pbnm$ (No. 62)] with $a < c/\sqrt{2} < b$,¹⁴ deviating from cubic only by a few percent ($[(b-a)/a < 5.5\%$). A thorough x-ray analysis was performed only for one example (LaScO₃), where a pole figure (111 reflection) indicates that the film crystallizes predominantly with the c axis normal to the substrate, with a much weaker component exhibiting an in-plane c axis. Scans through the film's 002, 224, 204, and 024 peaks are consistent with $a=5.72$ Å and

$b=5.80$ Å (in plane), and $c=8.11$ Å normal to the substrate. This orientation is different from that reported in Ref. 7 (c axis in the plane) for films on SrTiO₃ and MgO substrates.

The film thickness and optical band gap were determined by spectroscopic ellipsometry (SE) measurements using the two-modulator generalized ellipsometer¹⁵ (2-MGE) from 1.5 to 5.6 eV (840–220 nm) and a conventional fixed polarizer-sample-rotating polarizer system used under nitrogen ambient¹⁶ from 5 to 9 eV (250–140 nm). The data were fit using a four-media model: air/surface roughness/film/substrate. The thickness values obtained from the low-energy data are particularly accurate, with correlated errors better than 0.2% of the film thickness. The band gap is found from the intercept with the energy axis in a plot of α^2 versus photon energy for the high-energy data, where $\alpha=4\pi k/\lambda$ and λ is the wavelength. In all cases, α was in excess of 10^4 cm⁻¹ for almost all of the fitted range; absorption coefficients below 10^3 cm⁻¹ are difficult to determine accurately by SE. More details are found in Refs. 16 and 17.

The dielectric constants were measured at 1.7 GHz by evanescent-probe microwave microscopy,^{18,19} using a refined data analysis approach described elsewhere.²⁰ For these measurements, a sharp metallic tip, being part of a $\lambda/4$ resonator, is brought in contact with the sample (10 μ m contact area diameter, as determined by scanning electron microscopy after each series of measurements). The following resonance frequencies are measured (with a precision of 10–200 ppm): f_0 for the resonator without a sample, f_{sample} for the resonator in contact with each of the thin film samples, and $f_{substrate}$ for the resonator in contact with a bare LaAlO₃ substrate. This defines the values of $\Delta f/f(sample)=(f_{sample}-f_0)/f_{sample}$ and $\Delta f/f(substrate)=(f_{substrate}-f_0)/f_{substrate}$. Care is taken to measure $\Delta f/f(substrate)$ before and after each measurement of $\Delta f/f(sample)$ to guard against shifts in the background signal over the course of the experiment. Using the film thickness determined from ellipsometry, finite element calculations as described in Ref. 19 are used to calculate the frequency shift ratios $[\Delta f/f(sample)]/[\Delta f/f(substrate)]$ expected for different values of K , thus creating a lookup chart from which the films' K value is determined.

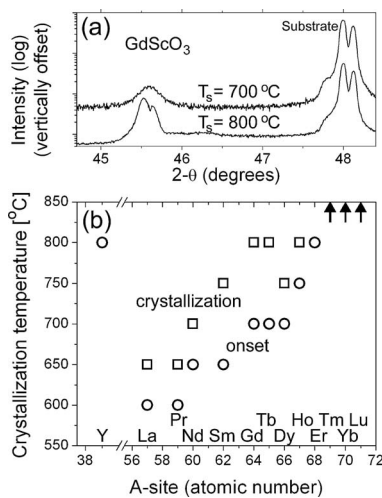


FIG. 1. (a) X-ray diffraction θ - 2θ scans through the film's pseudocubic 002 reflection and the $LaAlO_3$ substrate peak for the case of $GdScO_3$ films grown at two different temperatures. The sample grown at 700 °C shows the appearance of a broad film diffraction peak, defining $T_{onset}=700$ °C for this sample. At 800 °C, a clear separation into the $CuK\alpha_1$ and $CuK\alpha_2$ components is apparent (peak splitting); therefore $T_{cryst}=800$ °C. (b) Crystallization temperature as a function of the A-site atomic number for the entire series of scandates. Arrows indicate either a crystallization onset temperature above 800 °C or no formation of the perovskite phase.

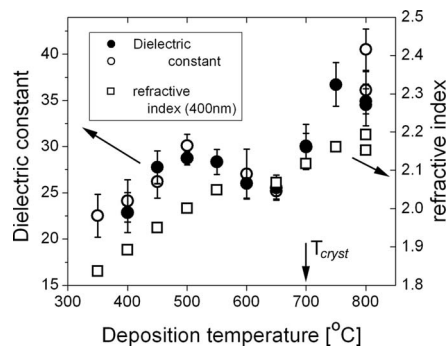


FIG. 2. Dielectric constant K at 1.7 GHz of NdScO_3 films deposited at different temperatures (circles, left-hand scale) and their refractive index at 400 nm. Open and solid circles refer to relative permittivities determined from background substrate measurements made before and after the films are measured, respectively, as described in the text. These are placed in the figure to demonstrate the reproducibility of the measurements.

The accuracy of the approach was checked by measurements of two compositions with significantly different film thicknesses, LaScO_3 and PrScO_3 . Any errors resulting from changes in tip geometry during the sequence of measurements or from numerical artifacts related to different film thicknesses would immediately result in different values of K being found for the samples of each pair. Excellent agreement (see Table I) was found.

To illustrate the dependence of the dielectric constant and of the refractive index on the deposition temperature, the results for the entire series of NdScO_3 samples are shown in Fig. 2. Clearly, a high value of $K \approx 36$ is obtained for well-crystallized samples (deposited above 700°C), while the amorphous samples exhibit a significantly lower $K \approx 25$. Note that these values are much larger than those for any binary oxide that is insulating, water insoluble, and stable in contact with Si ($K \approx 22$ for ZrO_2 and HfO_2).^{3,19}

Results of K for samples deposited at 800°C of all the scandates are shown in Fig. 3. With the exception of ErScO_3 ($Z=68$) and YScO_3 ($Z=39$), which are not fully crystallized at 800°C , no obvious dependence of K on the atomic number is observed. Comparing these results to bulk values, it is immediately observed that the films' K values are closest to the larger bulk values measured along the orthorhombic

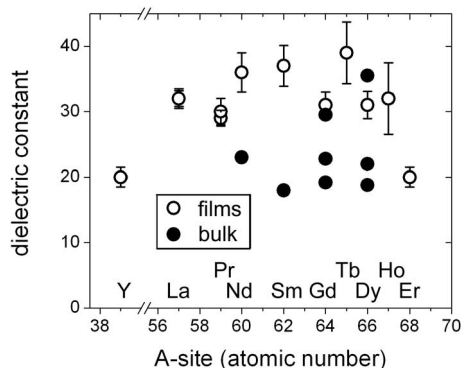


FIG. 3. Dielectric constant K at 1.7 GHz (right-hand scale) for the series of rare-earth scandates determined by microwave microscopy with the error bars representing the standard deviation of three measurements for each sample. For comparison, bulk dielectric constants (Ref. 3) (measured at 1 MHz) are shown as solid circles (multiple data points indicate the tensor coefficients along the principal axes for single-crystal measurements).

[001] direction, consistent with the electric field geometry in the microwave microscope^{19,21} and the assumption (based on the measurements for LaScO_3) that all films are oriented with their c axis perpendicular to the substrate.

Our comprehensive study of scandate films on LaAlO_3 substrates (Table I) provides the most complete set of data for epitaxial scandate films available. Low crystallization temperatures are found at compositions with a high Goldschmidt tolerance factor. Importantly, several scandate materials crystallize at fairly low temperatures ($\leq 700^\circ\text{C}$); the resulting crystalline scandates exhibit large optical band gaps (>5 eV) and high dielectric constants ($K > 30$), significantly larger than in their amorphous or poorly crystallized counterparts.

The authors gratefully acknowledge stimulating discussions with Jürgen Schubert. Research sponsored by the U.S. Department of Energy under Contract No. DE-AC05-00OR22725 with the Oak Ridge National Laboratory, managed by UT-Battelle, LLC. Y.J. and D.G.S. acknowledge the financial support of the Semiconductor Research Corporation (SRC) and SEMATECH through the SRC/SEMATECH FEP Center. E.C. and J.L.F. gratefully acknowledge financial support by the National Science Foundation under Grant No. 0218288.

¹D. G. Schlom and J. H. Haeni, MRS Bull. **27**, 198 (2002).

²J. B. Clark, P. W. Richter, and L. Du Toit, J. Solid State Chem. **23**, 129 (1978).

³D. G. Schlom, C. A. Billman, J. H. Haeni, J. Lettieri, P. H. Tan, R. R. M. Held, S. Völk, and K. J. Hubbard, in *Thin Films and Heterostructures for Oxide Electronics*, edited by S. B. Ogale (Springer, New York, 2005), pp. 31–78.

⁴S.-G. Lim, S. Kriventsov, T. N. Jackson, J. H. Haeni, D. G. Schlom, A. M. Balbashov, R. Uecker, P. Reiche, J. L. Freeouf, and G. Lucovsky, J. Appl. Phys. **91**, 4500 (2002).

⁵G. Lucovsky, Y. Zhang, J. L. Whitten, D. G. Schlom, and J. L. Freeouf, Microelectron. Eng. **72**, 288 (2004).

⁶G. Lucovsky, J. G. Hong, C. C. Fulton, Y. Zou, R. J. Nemanich, H. Ade, D. G. Schlom, and J. L. Freeouf, Phys. Status Solidi B **241**, 2221 (2004).

⁷T. Heeg, J. Schubert, C. Buchal, E. Cicerella, J. L. Freeouf, W. Tian, Y. Jia, and D. G. Schlom, Appl. Phys. A: Mater. Sci. Process. (in press).

⁸V. V. Afanas'ev, A. Stesmans, C. Zhao, M. Caymax, T. Heeg, J. Schubert, Y. Jia, D. G. Schlom, and G. Lucovsky, Appl. Phys. Lett. **85**, 5917 (2004).

⁹C. Zhao, T. Witters, B. Brijs, H. Bender, O. Richard, M. Caymax, T. Heeg, J. Schubert, V. V. Afanas'ev, A. Stesmans, and D. G. Schlom, Appl. Phys. Lett. **86**, 132903 (2005).

¹⁰I. Ohkubo, H. M. Christen, S. V. Kalinin, G. E. Jellison, Jr., C. M. Rouleau, and D. H. Lowndes, Appl. Phys. Lett. **84**, 1350 (2004).

¹¹K. J. Hubbard and D. G. Schlom, J. Mater. Res. **11**, 2757 (1996).

¹²K. L. Ovanesyan, A. G. Petrosyan, G. O. Shirinyan, C. Pedrini, and L. Zhang, Opt. Mater. (Amsterdam, Neth.) **10**, 291 (1998).

¹³M. D. Biegalski, J. H. Haeni, S. Trolrier-McKinstry, D. G. Schlom, C. D. Brandle, and A. J. Ven Graitis, J. Mater. Res. **20**, 952 (2005).

¹⁴R. P. Liferovich and R. H. Mitchell, J. Solid State Chem. **177**, 2188 (2004).

¹⁵G. E. Jellison, Jr. and F. A. Modine, Appl. Opt. **36**, 8184 (1997); **36**, 8190 (1997).

¹⁶E. Cicerella, J. L. Freeouf, L. F. Edge, D. G. Schlom, T. Heeg, J. Schubert, and S. A. Chambers, J. Vac. Sci. Technol. A **23**, 1676 (2005).

¹⁷G. E. Jellison, Jr., Thin Solid Films **234**, 416 (1993); **313–314**, 33 (1998).

¹⁸C. Gao and X. D. Xiang, Rev. Sci. Instrum. **69**, 3846 (1998).

¹⁹Y. G. Wang, M. E. Reeves, W. J. Kim, J. S. Horwitz, and F. J. Rachford, Appl. Phys. Lett. **78**, 3872 (2001).

²⁰M. E. Reeves (unpublished).

²¹Landolt-Börnstein: Numerical Data and Functional Relationships in Science and Technology, New Series, Group III, Vol. 7e, edited by K.-H. Hellwege and A. M. Hellwege (Springer, Berlin, 1976), pp. 11–13.